Resonant and non-resonant patterns in forced oscillations

Bradley Marts,[1] Aric Hagberg,[2] Ehud Meron,[3,4] and Anna L. Lin[1]

[1]*Department of Physics, Duke University, Durham, NC 27708*
[2]*Mathematical Modeling and Analysis, Theoretical Division, Los Alamos National Laboratory, Los Alamos, NM 87545*
[3]*Department of Solar Energy and Environmental Physics, BIDR, Ben Gurion University, Sede Boker Campus 84990, Israel*
[4]*Department of Physics, Ben-Gurion University, Beer Sheva 84105, Israel*

(Dated: September 28, 2006)

Uniform oscillations in spatially extended systems resonate with temporal periodic forcing within the Arnold tongues of single forced oscillators. The Arnold tongues are wedge-like domains in the parameter space spanned by the forcing amplitude and frequency, within which the oscillator's frequency is locked to a fraction of the forcing frequency. Spatial patterning can modify these domains. We describe here two pattern formation mechanisms affecting frequency locking at half the forcing frequency. The mechanisms are associated with phase-front instabilities and a Turing-like instability of the rest state. Our studies combine experiments on the ruthenium catalyzed light-sensitive Belousov-Zhabotinsky reaction forced by periodic illumination, and numerical and analytical studies of two model systems, the FitzHugh-Nagumo (FHN) model and the complex Ginzburg-Landau (CGL) equation, with additional terms describing periodic forcing.

PACS numbers: 05.45.Xt, 47.20.Ky, 47.54.+r

When a nonlinear oscillator is periodically forced by some external source, its oscillations can adjust and entrain to the forcing. The resulting dynamics is periodic with an oscillation frequency being a rational fraction of the forcing frequency. This entrainment, or frequency-locking, phenomenon occurs over a range of forcing frequencies and amplitudes, and is independent of the nature of the oscillators, which can be mechanical, electrical, chemical, or biological. Frequency locking exhibits many universal features and has been carefully studied for a variety of oscillator systems. Whether these universal features persist under conditions in which the oscillations are extended in space is the subject of our examination. We use an oscillatory chemical system spread in a thin gel layer, and two model systems, the FitzHugh Nagumo model and the complex Ginzburg-Landau equation, a generic equation for an oscillating field near the onset of oscillations, to explore how spatial extent change the universal properties of frequency locking. Our studies show that pattern formation can extend or reduce the range of frequency locking. Two pattern formation mechanisms responsible for such changes are identified, a phase-front instability designating a transition from standing-wave to traveling-wave dynamics, and a Turing-like instability inducing standing-wave patterns.

I. INTRODUCTION

Oscillatory dynamics have been observed in a variety of dissipative non-equilibrium systems including lasers, convective fluids, chemical reactions and cardiac tissues [1–4]. Among these systems, oscillating chemical reactions subjected to time-periodic forcing, have been particularly instrumental in exploring pattern formation phenomena [5, 6]. Experiments on the Belousov-Zhabotinsky reaction demonstrated a wide range of phenomena not normally seen in a single pattern forming system. These include traveling phase waves, Turing-like patterns, front instabilities leading to fingering and vortex-pair nucleation, spiral turbulence, and more [7, 8].

Oscillating systems often respond to periodic forcing by adjusting their oscillation frequencies to rational fractions of the forcing frequency [9]. This so called frequency-locking phenomenon is accompanied by another significant outcome of the periodic forcing - multiplicity of stable phase states [4]. Each phase state represents spatially uniform frequency-locked oscillations with a fixed oscillation phase. A well studied example is the 2:1 resonance where the system responds at exactly half the forcing frequency [10–12]. In this case there are two stable phase states whose oscillation phases differ by π. Along with the two uniform phase states, spatial front structures bi-asymptotic to the two states exist. Transverse instabilities and non-equilibrium Ising-Bloch (NIB) bifurcations of these front structures induce a variety of pattern formation phenomena. The 2:1 resonance exhibits yet another outcome of periodic forcing - a finite-wavenumber instability leading to standing-wave Turing-like patterns.

In the parameter plane spanned by the forcing frequency and forcing amplitude, spatially uniform resonant dynamics are confined to wedge-like domains, the so called Arnold Tongues [13, 14]. Are these resonance domains affected by the appearance of stationary or time-dependent patterns? In this paper we address this question in the context of the 2:1 resonance [15]. We review pattern formation mechanisms associated with front instabilities and Turing instabilities, and examine the power spectra of the time signals for the resulting dynamics. Our studies involve experiments on the ruthenium catalyzed light-sensitive [16, 17] Belousov-Zhabotinsky (BZ) reaction, periodically forced in time with spatially uniform light, and numerical studies of two model systems, the FitzHugh-Nagumo (FHN) model and the complex Ginzburg-

Landau (CGL) equation, with additional terms describing periodic forcing.

II. THE BZ EXPERIMENT

The BZ reaction takes place in a reactor system containing a thin porous Vycor glass membrane that is 0.4 mm thick and 22 mm in diameter. Typical chemical patterns observed in the membrane have length scales of 0.5 mm or greater and are effectively two-dimensional. Reagents diffuse homogeneously from continuously stirred reservoirs into the glass through its two faces. We image the reaction by passing spatially homogeneous low-intensity light through the membrane, and measure the relative intensity of the transmitted light using a CCD camera bandpass filtered at 451 nm, the peak absorption frequency of the ruthenium catalyst. Regions of the membrane that contain a high concentration of Ru(II) pass low intensity light to the camera; regions that contain a low concentration pass a higher intensity.

We periodically perturb the light-sensitive BZ oscillatory reaction with light of different intensities and pulse frequencies to investigate the existence, shape and extent of Arnold tongues in a spatially extended oscillatory system [18]. We find regions of resonance in the forcing parameter plane, see Fig. 1, ordered in the Farey sequence of rational numbers, a signature of the resonance domains studied by Arnold and others. These experimental resonance domains also exhibit fundamental differences –in particular, in the breadth of resonance in the frequency dimension, and in the extent of resonance observed in the amplitude dimension. The range of resonance is both extended and diminished through pattern formation. We explore various mechanisms in the context of the 2:1 resonance domain.

III. MODEL SYSTEMS

A. The forced FitzHugh-Nagumo model

As a model for a periodically forced oscillatory system we use the FitzHugh-Nagumo (FHN) reaction-diffusion equations modified to include time-periodic forcing

$$u_t = u - u^3 - v + \nabla^2 u\,, \tag{1a}$$
$$v_t = \epsilon\left[u - a_1 v - a_0 + \Gamma v \sin(\omega_f t)\right] + \delta\nabla^2 v\,. \tag{1b}$$

Here $u(x,y)$ and $v(x,y)$ are scalar fields representing the concentrations of activator and inhibitor types of chemical reagents. The periodic forcing is assumed to be sinusoidal with amplitude Γ and frequency ω_f. The parameter ϵ is the ratio of the characteristic time scales of u and v and δ is the ratio of the diffusion rates of u and v.

In the absence of forcing, $\Gamma = 0$, Eqs. (1) have a spatially uniform solution $(u_0,\ v_0)$. This solution losses stability in a Hopf bifurcation to uniform oscillations as the parameter ϵ is decreased below a critical value ϵ_c. For the symmetric model ($a_0 = 0$) $\epsilon_c = 1/a_1$ and the Hopf frequency is $\omega_0 = \sqrt{1/a_1 - 1}$. Beyond the Hopf bifurcation (i.e. below ϵ_c) Eqs. (1) also support traveling phase waves.

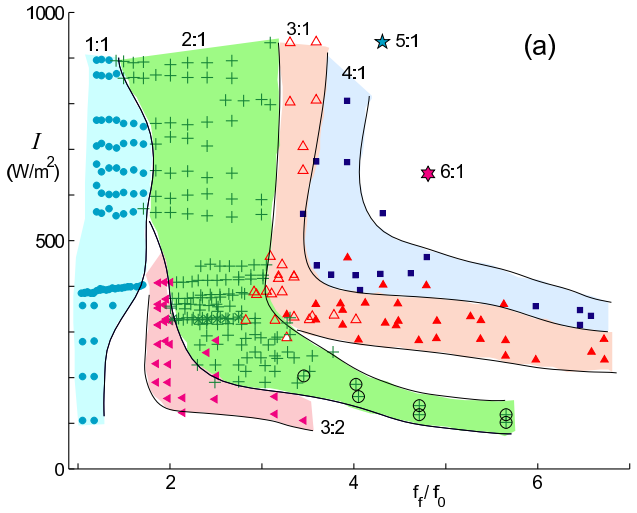

FIG. 1: The largest m:n tongues observed in the spatially extended BZ system. Each symbol type represents a different m:n response and a different spatial pattern. The patterns (points) within the solid curves respond sub-harmonically with the forcing frequency. The homogeneous oscillation frequency is $f_0 = 0.020$ Hz. The chemical conditions are given in [19].

Forcing the system at a frequency $\omega_f \approx 2\omega_0$ either leads to quasi-periodic oscillations or, when the forcing is strong enough, to periodic oscillations at a frequency $\omega = \omega_f/2$. The latter case corresponds to 2:1 frequency-locked oscillations where the system adjusts its oscillation frequency to $\omega = \omega_f/2$ despite the fact that $\omega_0 \neq \omega_f/2$. Fig. 2 shows a numerical computation of the 2:1 resonance boundaries (Arnold tongue) for uniform oscillations, above which frequency locking takes place.

B. The forced complex Ginzburg-Landau equation

Near the Hopf bifurcation, where the oscillation amplitude is small, the u and v fields can be approximated by

$$u \approx u_0 + \left[A e^{i\frac{\omega_f}{2}t} + c.c.\right]\,, \tag{2a}$$
$$v \approx v_0 + \left[\zeta A e^{i\frac{\omega_f}{2}t} + c.c.\right]\,, \tag{2b}$$

where A is a complex-valued amplitude, slowly varying in space and time. For weak forcing, the amplitude A satisfies the complex Ginzburg-Landau equation [20–23],

$$A_t = (\mu + i\nu)A + (1+i\alpha)\nabla^2 A - (1+i\beta)|A|^2 A + \gamma A^*\,. \tag{3}$$

The term A^* in this equation is the complex conjugate of A and describes the effect of the weak periodic forcing [20]. The parameter μ represents the distance from the Hopf bifurcation, $\nu = \omega_0 - \omega_f/2$ is the detuning, α represents dispersion, β represents nonlinear frequency correction, and γ represents the forcing amplitude (proportional to Γ). Exact forms for

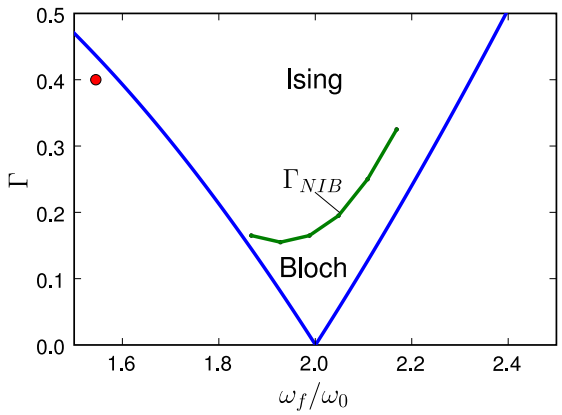

FIG. 2: The resonance tongue boundaries for the 2:1 response of the periodically forced FHN equations (1). The horizontal axis spans the ratio of the forcing frequency ω_f to the Hopf frequency, $\omega_0 \approx 0.83$, of the unforced system. Within the tongue boundaries the system oscillates at exactly half the forcing frequency. The green curve marked as Γ_{NIB} is the NIB boundary; above are stationary Ising patterns and below are traveling Bloch wave patterns. The red circle marks the parameter values of standing waves found outside the resonance tongue. The parameters in the FHN equations are $\epsilon = 1$, $\delta = 4.0$, $a_1 = 0.5$, $a_0 = 0.1$.

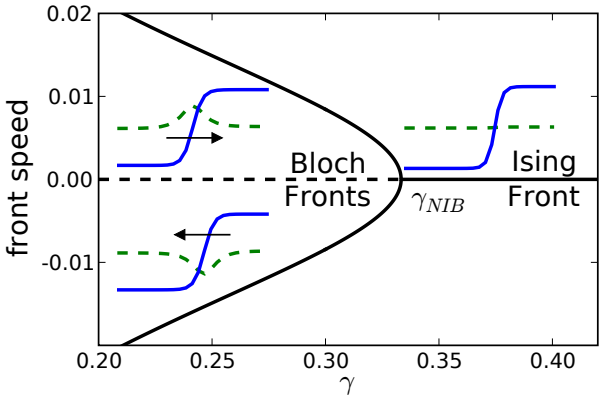

FIG. 3: The nonequilibrium Ising-Bloch (NIB) bifurcation for the forced CGL equation (3). For $\gamma > \gamma_c$ there is a single stable Ising front with zero speed. For $\gamma < \gamma_c$ the Ising front is unstable and there are a pair of stable counter-propagating Bloch fronts. The insets show the shape of $\mathrm{Re}(A)$ (solid blue curve) and $\mathrm{Im}(A)$ (dashed green curve) across the front position. Parameters: $\mu = 1.0$, $\nu = 0.01$, $\beta = \alpha = 0.0$.

these parameters have been derived for specific models such as the Brusselator and the FHN models [24, 25].

According to Eqs. (2) stable stationary solutions of the amplitude equation (3) describe frequency-locked or resonant oscillations. Uniform solutions of this kind exist for $\gamma > \gamma_b$ where [26]

$$\gamma_b = \frac{|\nu - \mu\beta|}{\sqrt{1+\beta^2}}\,. \tag{4}$$

In the next two sections we show that non-uniform solutions may restrict or extend the boundaries of resonant response.

IV. NON-RESONANT FRONT DYNAMICS

A. The NIB bifurcation

Within the tongue boundaries, γ_b, of the 2:1 resonance, front structures shifting the oscillation phase by π exist. We use the forced CGL equation (3) to study the corresponding front solutions. We recall that stationary solutions of Eq. (3) correspond to resonant oscillations at $\omega_f/2$. Resonant oscillations are therefore destroyed when front dynamics set in; the oscillation frequency at a given point changes when a moving front is passing by. One mechanism which induces front dynamics is the non-equilibrium Ising-Bloch (NIB) bifurcation. This is a pitchfork bifurcation in which a stationary "Ising front" loses stability to a pair of counter-propagating "Bloch fronts" as the forcing strength decreases below a threshold γ_{NIB}. A NIB bifurcation diagram for Eq. (3) is shown in Fig. 3. For the special case $\alpha = \beta = 0$, the threshold is given

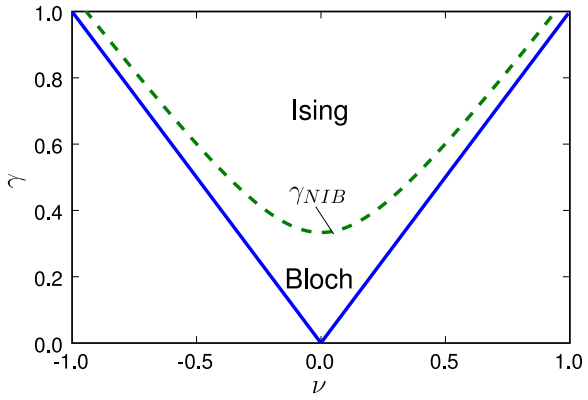

FIG. 4: Resonance tongue diagram for the FCGL equation (3). Inside the tongue-shaped region bounded by the solid lines $\gamma = |\nu|$ (for $\beta = 0$) uniform solutions are frequency-locked (resonant). Above the dashed curve $\gamma = \gamma_{NIB}$ resonant standing wave patterns (stripes, labyrinths, and spots) are found while below γ_{NIB} non-resonant Bloch-front spiral waves prevail.

by [27]

$$\gamma_{NIB} = \sqrt{\nu^2 + (\mu/3)^2}\,. \tag{5}$$

Figure 4 shows the tongue boundaries of the 2:1 resonance, calculated from Eq. (4), and the NIB bifurcation threshold (5). The NIB threshold splits the 2:1 resonance tongue into two parts, a Bloch part, $\gamma_b < \gamma < \gamma_{NIB}$, and an Ising part, $\gamma > \gamma_{NIB}$. When α is nonzero and positive (negative) the NIB boundary ($\gamma = \gamma_{NIB}$) shifts to the right (left) tongue boundary. The NIB boundary for the FHN model is shown in Fig. 2.

In one space dimension, the NIB bifurcation threshold designates a sharp transition from resonant stationary Ising patterns at high forcing strengths, to non-resonant traveling

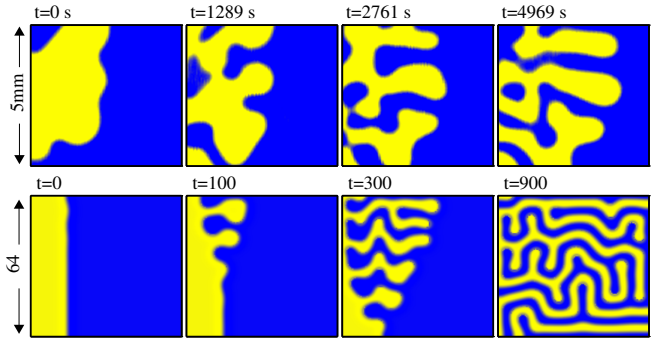

FIG. 5: Formation of labyrinthine patterns by transverse front instability. The interface between the two oscillation phases is transversely unstable and small perturbations grow and finger. (top) Patterns from a region of the BZ reactor, strobed at half the forcing frequency. Blue (yellow) represents regions of low (high) Ru(III) concentration. (bottom) Patterns in the FCGL equation (3). Blue and yellow regions are different phases separated by π. Parameters: $\gamma = 2.02$, $\mu = 1$, $\nu = 2.0$, $\alpha = 0.5$, $\beta = 0$.

Bloch waves at low forcing strengths [12, 28]. In two space dimensions the transition is not necessarily sharp; an intermediate range of turbulent dynamics can appear in the vicinity of the NIB boundary when a transverse front instability develops.

B. Bloch-front turbulence

Ising and Bloch fronts in bistable systems can go through transverse front instabilities [29]. Far into the Ising regime transverse instabilities often lead to stationary labyrinthine patterns through fingering and tip splitting. Close to the NIB bifurcation they may induce turbulent states involving repeated events of spiral-vortex nucleation and annihilation (hereafter Bloch-front turbulence or BFT) [8].

In the context of forced oscillations, transverse instabilities of Ising fronts have been studied both theoretically, using Eq. (3) [26] and in experiments on the BZ reaction [30]. Fig. 5a shows experimental results demonstrating a transverse front instability. Fig. 5b shows a numerical demonstration of a transverse instability and the fingering and tip splitting processes that lead to a resonant labyrinthine pattern in the Ising regime far from the NIB bifurcation. Another typical resonant behavior in this parameter regime is the appearance of localized spot-like structures close to the transverse instability threshold [31, 32].

As the NIB bifurcation is approached the dynamics change; instead of fingering and tip splitting, growing transverse perturbations now induce vortex nucleation followed by a non-resonant state of Bloch-front turbulence as Figs. 6 and 7 show. Far into the Bloch regime stable non-resonant spiral waves prevail. Figure 8(a)-(c) summarizes the qualitative spatio-temporal behaviors as the NIB bifurcation is traversed. For comparison we show in Fig. 8(d)-(f) the corresponding behaviors in the absence of a transverse instability. In that case the NIB bifurcation designates a sharp transition between non-resonant traveling waves below γ_{NIB} to resonant large domain patterns above γ_{NIB}. Approaching the NIB bifurcation from below leads to a spiral wave with a diverging pitch and vanishing rotation speed.

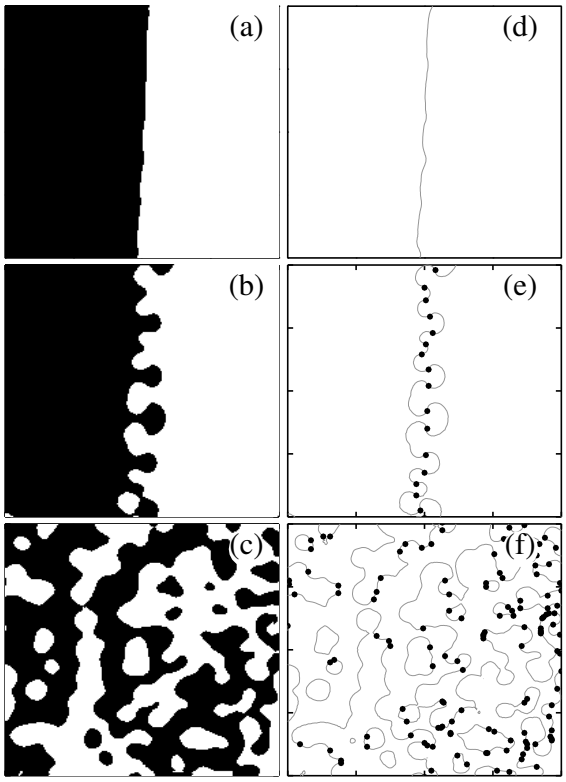

FIG. 6: Spiral vortex nucleation in the BZ system. Frames (a)-(c) show the phase of the oscillations at near half the driving frequency at three different times $t = 100s, 300s, 1700s$ [33]. Frames (d)-(f) show the position of the vortices along the front at the corresponding times. (a) The initial nearly planar front is unstable to transverse perturbations. (b) Vortices form in pairs along the front. (c) Vortices eventually fill up the entire system. The figures show a 19.1 mm $\times$ 19.1 mm (200 $\times$ 200 pixel) region of the BZ system with the light forcing intensity $I = 165$ W/m^2, uniform oscillation frequency of $f_0 = 0.02$ Hz, and forcing frequency of $f_f = 0.06$ Hz. Chemical conditions are given in Ref. [34].

C. Kinematic equations for Bloch spirals and vortex nucleation

Bloch spiral waves and spontaneous spiral-vortex nucleation leading to BFT can be studied using a kinematic approach for the dynamics of curved fronts. The normal form equations for a curved front in the vicinity of the NIB bifurcation are [35]:

$$\frac{d\kappa}{dt} = -(\kappa^2 + \frac{\partial^2}{\partial s^2})C_n \,, \tag{6a}$$

$$\frac{dC_0}{dt} = (a_{nib} - a)C_0 - bC_0^3 + c\kappa + \frac{\partial^2 C_0}{\partial s^2} \,, \tag{6b}$$

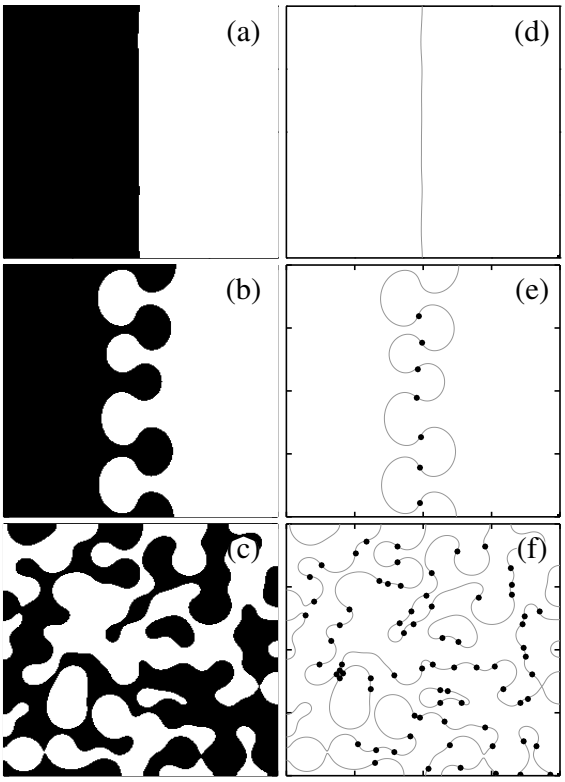

FIG. 7: Spiral-vortex nucleation and formation of Bloch-front turbulence in a numerical solution of the CGL equation (3). Frames (a)-(c) show the phase $arg(A)$ of the solution at three different times t=180,800,8000. Perturbations on the unstable front solution grow and pairs of vortices form along the front. Frames (d)-(f) show the same data but with the vortices shown as solid dots along the front. The front is defined as $Re(A) = 0$ and the vortex positions are where in addition $Im(A) == 0$. Parameters used were $\mu = 0.5, \nu = 0.15$, $\alpha = 0.3$, $\beta = 0$, $\gamma = 0.2$ on a domain size of $[x, y] = [256, 256]$ with no-flux boundary conditions.

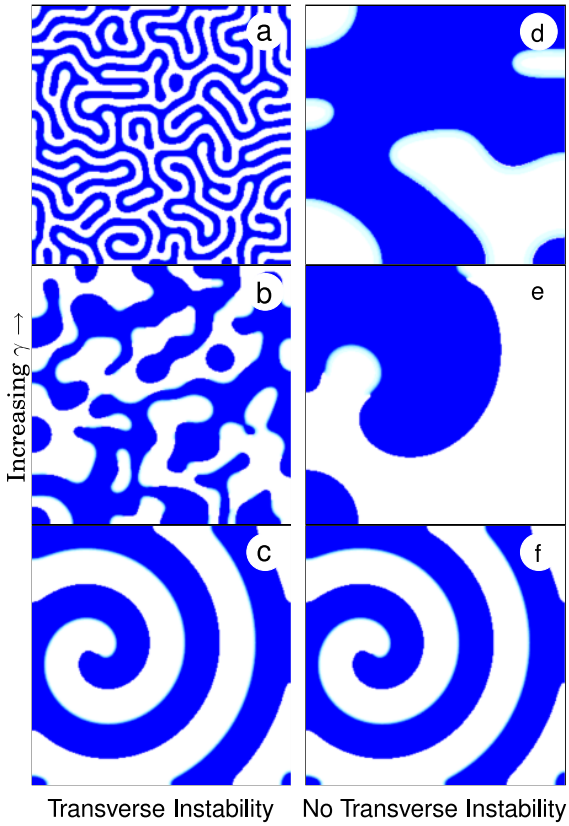

FIG. 8: Contrasting pattern formation phenomena in the CGL equation (3) as the parameters are varied across the NIB bifurcation. Far below the NIB threshold stable Bloch spirals prevail [panels (c) and (f)] . As the forcing amplitude is increased two scenarios are possible, depending on whether the Bloch and Ising fronts are unstable (left column) or stable (right column) to transverse perturbations. When a transverse front instability exists a state of Bloch-front turbulence first appears (b), followed by labyrinthine Ising patterns (a). When the fronts are transversly stable a sharp transition from Bloch spirals to large-domain Ising patterns (d) takes place across the NIB bifurcation, with the Bloch-spiral pitch increasing indefinitely as the NIB threshold is approached (e). Parameters: $\mu = 0.5$,$\alpha = 0.35$, $\beta = 0$ and (a) Ising Labyrinth: $\nu = 0.38$, $\gamma = 0.4$; (b) BFT: $\nu = 0.14$, $\gamma = 0.2$; (c) Bloch spiral: $\nu = 0.14$, $\gamma = 0.15$; (d) Ising large domains: $\nu = 0.15$, $\gamma = 0.3$; (e) Bloch spiral near NIB:$\nu = 0.08, \gamma = 0.15$; (f) Bloch spiral: $\nu = 0.14, \gamma = 0.15$; The integration domain was $[x, y] = [256, 256]$ and no-flux boundary conditions were used.

where C_n, the normal front velocity, is related to C_0, the velocity of a planar front, through the relation, $C_n = c_0 - D\kappa$, s is arclength, and $\frac{d}{dt}$ is the total time derivative: $\frac{d}{dt} = \frac{\partial}{\partial t} + \frac{ds}{dt}\frac{\partial}{\partial s}$. The arclength changes in time, when the front is curved and moving, according to $\frac{ds}{dt} = \int_0^s \kappa C_n ds'$.

Equations (6) capture the NIB bifurcation for a planar front as the bifurcation parameter a crosses the threshold a_{nib}; an Ising front solution, $(C_0, \kappa) = (0, 0)$, loses stability and two stable Bloch front solutions, $(C_0, \kappa) = (\pm\sqrt{a_{nib} - a)/b}, 0)$, appear. In the Bloch regime ($a < a_{nib}$) Eqs. (6) admit a kink solution bi-asymptotic (as $|s| \to \infty$) to the two Bloch front solutions as Fig. 9(a) shows. In the two-dimensional $x - y$ plane this kink solution describes a rotating spiral wave [Fig. 9(b)].

Figures 10 and 11 show the dynamics of a closed front loop that contains a vortex pair in the Bloch regime (Fig. 10) and in the Ising regime (Fig. 11). The simulations were done on a version of Eqs. (6) suitable for describing the dynamics of closed loops [36]. In the Bloch regime the two vortices converge to a pair of counter-rotating spiral waves, while in the Ising regime mutual vortex annihilation leads to a circular Ising front whose speed becomes vanishingly small as it expand outwards.

Equations (6) also imply that Bloch fronts close to the NIB bifurcation are unstable to transverse perturbations provided $c/D > 0$ [37]. To see this we study the stability of planar Bloch fronts to perturbations of the form $(\delta C_0, \delta\kappa) \exp(\sigma t + iQs) + c.c.$. Inserting the perturbed forms for C_0 and κ in Eqs. (6) gives the neutral stability ($\sigma = 0$) relation

$$a_{tr}(Q) = a_{nib} - \frac{c}{2D} + Q^2 . \qquad (7)$$

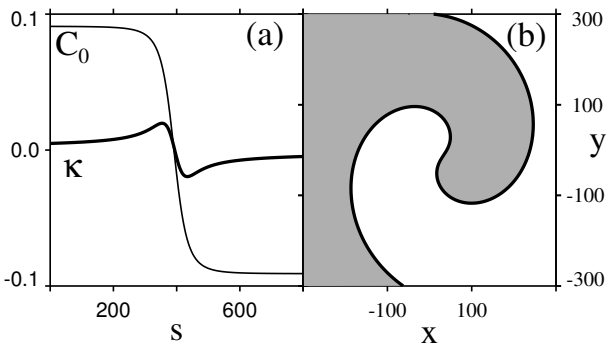

FIG. 9: Spiral wave solution of the kinematic equations (6). (a) The normal front velocity C_0 and curvature κ have a kink solution bi-asymptotic to the two Bloch fronts as the arclength $|s| \to \infty$. (b) In the $x - y$ (laboratory) coordinate frame the kink solution is a spiral wave. Parameters: $a = 5.99$, $a_{nib} = 6.0$, $b = 0.17$, $c = 6.0$.

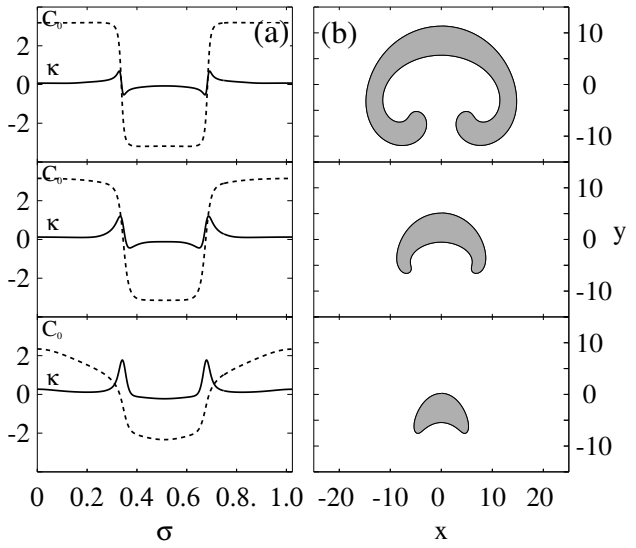

FIG. 10: Formation of a pair of spiral waves in the Bloch regime. (a) Solutions to the kinematic equations for closed loops [36] at $t = 0$ (bottom), $t = 2$ (middle), and $t = 4$ (top). The variable σ is the ratio of the arclength to the total loop length. (b) The corresponding solutions in the $x - y$ plane. Parameters: $\epsilon = 0.035$, $\delta = 1.1$, $a_0 = 0$, $a_1 = 2$, $d = 0$.

The first mode to grow is the zero mode, $Q = 0$. Within the range $a_{nib} - \frac{c}{2D} < a < a_{nib}$ Bloch fronts are unstable to transverse perturbations. As a approaches the NIB bifurcation threshold, a_{nib}, modes with higher and higher wave-numbers grow. When the curvature perturbations produced by these modes are sufficiently large, local transitions between the two Bloch fronts are induced and vortex nucleation events take place [38] as demonstrated in Fig. 12.

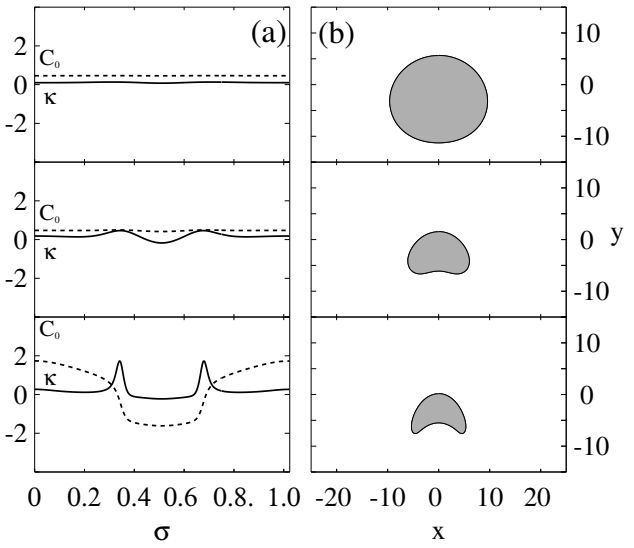

FIG. 11: Formation of an expanding circular loop in the Ising regime. (a) Solutions to the kinematic for closed loops [36]. at $t = 0$ (bottom), $t = 3$ (middle), and $t = 15$ (top). (b) The corresponding solutions in the $x - y$ plane. Parameters: $\epsilon = 0.14$, $\delta = 1.1$, $a_0 = 0.1$, $a_1 = 2$, $d = 0$.

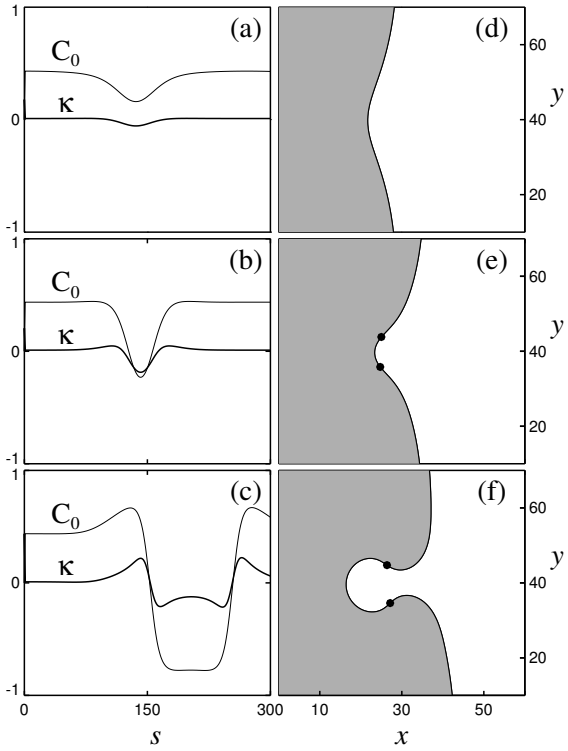

FIG. 12: Nucleation of a spiral-vortex pair in the kinematic equations (6). (a),(d) A small perturbation in the curvature grows. (b),(e) A portion of the domain reverses direction and a spiral-vortex pair nucleates along the front. (c),(f) A pair of rotating spiral-waves forms. Parameters: $a = 5.97$, $a_{nib} = 6.0$, $b = 0.165$, $c = 6.03$.

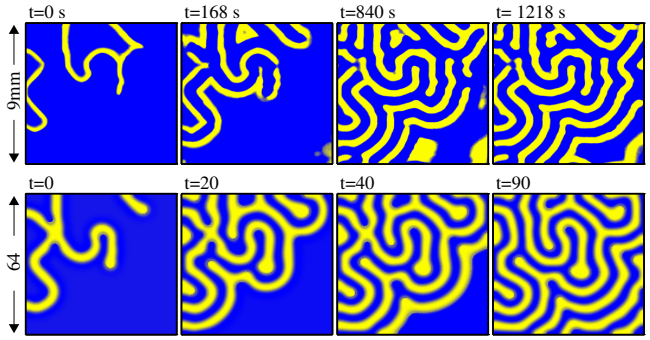

FIG. 13: Resonant standing waves invading non-resonant quasi-periodic oscillations. (top) Patterns from a region of the BZ reactor, strobed at half the forcing frequency. Blue (yellow) represents regions of low (high) Ru(III) concentration. (bottom) Patterns in the FCGL equation (3). Blue and yellow regions are different phases separated by π. Parameters: $\gamma = 1.98$, $\mu = 1$, $\nu = 2.0$, $\alpha = 0.5$, $\beta = 0$.

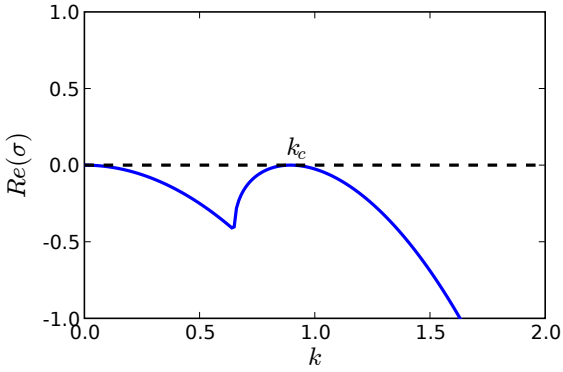

FIG. 14: The growth rate (real part of σ) of perturbations from the $A = 0$ state of Eq. (3) at the codimension 2 point, $\mu = 0$, $\gamma = \gamma_c$. Two modes become marginal at this point, a Hopf zero-k mode and a Turing finite-k mode. Parameters: $\mu = 0$, $\nu = 2.0$, $\alpha = 0.5$, $\gamma = \gamma_c \approx 1.8$.

V. RESONANCE INVASION

The NIB bifurcation is a mechanism by which resonant standing-wave patterns destabilize to non-resonant traveling waves. Figure 13 shows an experimental demonstration of an opposite behavior where non-resonant traveling waves are displaced by resonant standing-wave patterns. The mechanism of this behavior is associated with the appearance of a Turing mode [39] and has been studied by Yochelis et al. [26, 40]. Consider the dispersion relation associated with the zero state of Eq. 3 [30]:

$$\sigma = \mu - k^2 + \sqrt{\gamma^2 - (\nu - \alpha k^2)^2}\,. \tag{8}$$

An examination of this relation reveals a codimension two point,

$$\mu = 0, \quad \gamma = \gamma_c = \nu/\sqrt{1+\alpha^2}\,, \tag{9}$$

where the Hopf bifurcation to uniform oscillations coincides with a Turing instability [30], as Fig. 14 shows. The Hopf frequency and the Turing wavenumber are given by $\omega_0 = \nu\alpha/\rho$ and $k_0^2 = \nu\alpha/\rho^2$, respectively, where $\rho = \sqrt{1+\alpha^2}$. In the vicinity of the codimension 2 point, where $|\gamma - \gamma_c| \sim \mu \ll \gamma_c$, solutions of Eq. (3) can be approximated as

$$\begin{pmatrix} \mathrm{Re}\, A \\ \mathrm{Im}\, A \end{pmatrix} = \left\{ \mathbf{e_0} B_0 e^{i\omega_0 t} + \mathbf{e_k} B_k e^{ik_0 x} + c.c. \right\} + \cdots\,, \tag{10}$$

where the complex amplitudes $B_0(\mu t)$ and $B_k(\mu t)$ in Eq. (10) are of order $\sqrt{\mu}$, and describe slow uniform modulations of the (relatively) fast oscillations associated with the Hopf mode and of the fast spatial variations associated with the Turing mode. We refer the reader to Yochelis et al. [26] for the derivation of the normal form equations for the amplitudes B_0 and B_k, the so called Hopf-Turing amplitude equations. These equations have been studied in various contexts [41–47] and are known to have a parameter regime where stable uniform oscillations coexist with a stable Turing pattern.

In the present context, the uniform oscillations states pertain to non-resonant quasiperiodic oscillations, whereas the Turing-pattern state describes resonant standing waves. The range of bistability occurs outside the 2:1 resonance tongue and is bounded on one side by the tongue boundary. Moreover, close to the tongue boundary the Turing-pattern state invades the uniform-oscillations state as shown in Fig. 13(b). These findings explain the experimental observations shown in Fig. 13(a). Indeed, the displacement of traveling-wave state by the resonant standing-wave state has been observed in the vicinity of the tongue boundary.

The phenomenon of resonance invasion presented above has been predicted using an amplitude equation approach [Eq. (3)] [26, 30]. To test this prediction we studied resonance invasion in the FHN model (1). Figure 15(top) shows snapshots of a standing-wave pattern invading uniform oscillations outside the tongue boundary (parameters at solid circle in Fig. 2). Typical timeseries in the standing-wave and uniform-oscillations domains are shown in the middle part of Fig. 15, and the corresponding power spectra in the bottom part. While the uniform oscillations are quasi-perioic and unlocked to the forcing, the standing waves are clearly resonant, locked to half the forcing frequency.

VI. CONCLUSION

We described here joint theoretical and experimental studies of pattern formation mechanisms that affect the resonant response of oscillatory systems to periodic forcing. We focused on the 2:1 resonance case and highlighted two mechanisms. The first is associated with the NIB front bifurcation within the resonance tongue of uniform oscillations. The bifurcation restricts the range of resonant non-uniform oscillations to the Ising regime where phase fronts are stationary. The NIB bifurcation designates a sharp transition from non-resonant traveling waves to resonant standing waves when the phase fronts are transversely stable. In the presence of a trans-

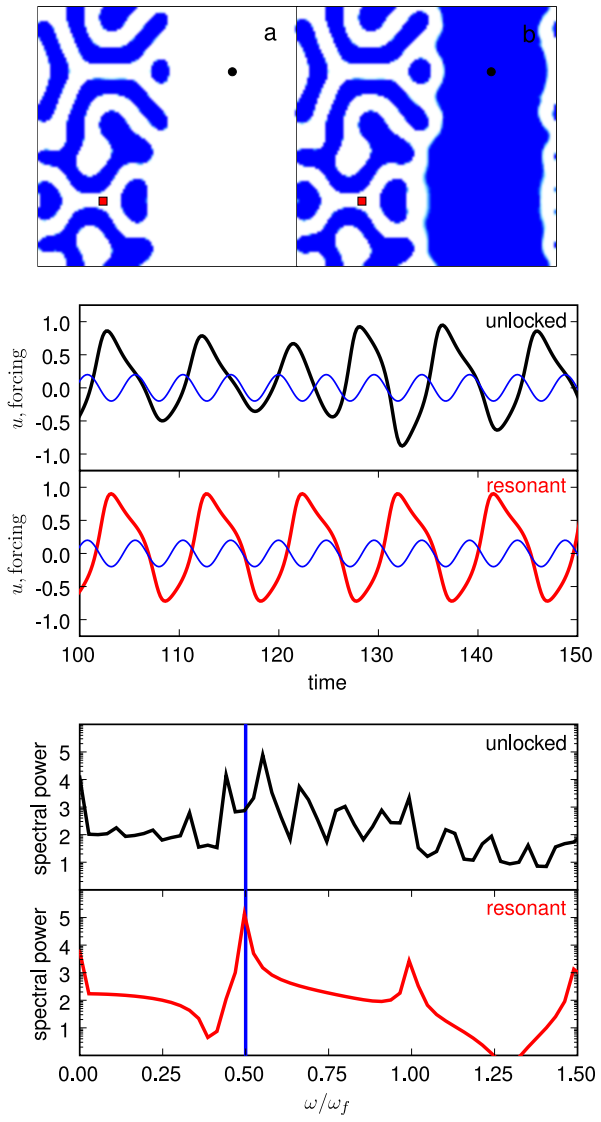

FIG. 15: A resonant pattern invading an unlocked oscillatory state in the forced FHN model (1). The parameters correspond to the point indicated by the solid circle on the tongue diagram in Fig. 2 ($\omega_f = 1.3$, $\Gamma = 0.4$. (top) Two snapshots in time of the pattern phase. The left half of the domain is resonant and the right half is unlocked with uniform oscillations. (middle) Timeseries for the two points shown in the top figure. The timeseries for the point at the black circle is not locked to the forcing (shown in the small sine wave). The timeseries at the red square is locked to the forcing and shows one full wavelength response for every two forcing wavelengths. (bottom) The power spectra of the two timeseries showing that the resonant part of the pattern is locked to 1/2 the forcing frequency as indicated by the vertical line.

verse front instability, an intermediate range of Bloch-front turbulence further restricts the range of resonant oscillations. A second mechanism affecting resonant response is associated with the appearance of a finite-wavenumber or Turing-like instability of the zero state. The instability is induced by the periodic forcing and can lead to the coexistence of stable non-resonant oscillations with stable resonant standing waves. Invasion of the latter state into the former leads to resonant response outside the Arnold tongue boundaries of uniform oscillations.

Equivalent mechanisms may work in other resonance tongues. Theoretical studies of the 4:1 resonance [22, 23], for example, revealed a front instability that designates a transition from resonant two-phase standing waves at high forcing strengths to non-resonant four-phase traveling waves at low forcing strengths. Like the NIB bifurcation, this front instability restricts the parameter range of non-uniform resonant oscillations within the 4:1 tongue.

Acknowledgements

We acknowledge the contributions of our collaborators, Arik Yochelis, Christian Elphick and Harry Swinney, to some of the studies reviewed here. This work was carried out under the auspices of the National Nuclear Security Administration of the U.S. Department of Energy at Los Alamos National Laboratory under Contract No. DE-AC52-06NA25396. Support was provided by the DOE Office of Science Advanced Scientific Computing Research (ASCR) Program in Applied Mathematics Research and NSF Grant DMR-0348910.

[1] M. C. Cross and P. C. Hohenberg, Rev. Mod. Phys. **65**, 851 (1993).

[2] C. Godreche and P. Manneville, *Hydrodynamics and Nonlinear Instabilities*, Cambridge University Press, 1998.

[3] I. R. Epstein and J. A. Pojman, *An Introduction to Nonlinear Chemical Dynamics : Oscillations, Waves, Patterns, and Chaos*, Topics in Physical Chemistry, Oxford University Press, 1998.

[4] A. Pikovsky, M. Rosenblum, and J. Kurths, *Synchronization: A Universal Concept in Nonlinear Sciences*, Cambridge University Press, 2001.

[5] V. Petrov, Q. Ouyang, and H. L. Swinney, Nature **388**, 655 (1997).

[6] V. K. Vanag, A. M. Zhabotinsky, and I. R. Epstein, Phys. Rev. Lett. **86**, 552 (2001).

[7] A. L. Lin et al., Phys. Rev. Lett. **84**, 4240 (2000).

[8] B. Marts, A. Hagberg, E. Meron, and A. L. Lin, Phys. Rev. Lett. **93**, 108305 (2004).

[9] J. M. T. Thompson and H. B. Stewart, *Nonlinear Dynamics and Chaos*, Wiley, 1986.

[10] P. Coullet, J. Lega, B. Houchmanzadeh, and J. Lajzerowicz, Phys. Rev. Lett. **65**, 1352 (1990).

[11] P. Coullet and K. Emilsson, Physica D **61**, 119 (1992).

[12] C. Elphick, A. Hagberg, E. Meron, and B. Malomed, Phys. Lett. A **230**, 33 (1997).

[13] V. I. Arnold, Izv. Akad. Nauk SSSR Ser. Mat. **25**, 21 (1961).

[14] V. I. Arnold, Usp. Mat. Nauk **38**, 189 (1983), English translation: Russian Math. Surveys 38 (1983), no. 4, 215–233.

[15] H.-K. Park, Phys. Rev. Lett. **86**, 1130 (2001).

[16] S. Kádár, T. Amemiya, and K. Showalter, J. Phys. Chem. **101**, 8200 (1997).

[17] K. Martinez, A. L. Lin, R. Kharrazian, X. Sailer, and H. L. Swinney, Physica D **168-169**, 1 (2002).

[18] A. L. Lin, A. Hagberg, E. Meron, and H. L. Swinney, Phys. Rev. E **69**, 066217 (2004).

[19] The chemical concentrations in the two chemical reserviors separated by the porous membrane were, Reservior I: 0.220 M bromo-malonic acid, 0.230 M potassium bromate, 0.80 M sulfuric acid; Reservior II: 0.184 M potassium bromate, 1×10^{-3} M Tris(2,2'-bipyridyl)dichlororuthenium(II)hexahydrate, 0.80 M sulfuric acid. Each reservior volume is 8.3 ml and the flow rate of chemicals through Reservior I was 20 ml/hr while through Reservior II it was 5 ml/hr. Chemicals were premixed before entering each reservior; a 10 ml premixer and a 0.5 ml premixer fed Reservior I and II, respectively. The experiments were conducted at room temperature.

[20] J. M. Gambaudo, J. Diff. Eq. **57**, 172 (1985).

[21] C. Elphick, G. Iooss, and E. Tirapegui, Phys. Lett. A **120**, 459 (1987).

[22] C. Elphick, A. Hagberg, and E. Meron, Phys. Rev. Lett. **80**, 5007 (1998).

[23] C. Elphick, A. Hagberg, and E. Meron, Phys. Rev. E **59**, 5285 (1999).

[24] Y. Kuramoto, *Chemical Oscillations, Waves, and Turbulence*, Springer Series in Synergetics, Springer-Verlag, 1984.

[25] C. J. Hemming, *Resonantly Forced Oscillatory Reaction-Diffusion Systems*, PhD thesis, University of Toronto, 2003.

[26] A. Yochelis, C. Elphick, A. Hagberg, and E. Meron, Physica D **199**, 201 (2004).

[27] D. V. Skryabin et al., Phys. Rev. E **64**, 056618 (2001).

[28] Note that uniform oscillations in the range $\gamma_b < \gamma < \gamma_{NIB}$ remain resonant and coexist with non-resonant Bloch waves.

[29] A. Hagberg and E. Meron, Chaos **4**, 477 (1994).

[30] A. Yochelis, A. Hagberg, E. Meron, A. L. Lin, and H. L. Swinney, SIADS **1**, 236 (2002).

[31] D. Gomila, P. Colet, G. L. Oppo, and M. S. Miguel, Phys. Rev. Lett. **87**, 194101 (2001).

[32] B. Marts, K. Martinez, and A. L. Lin, Phys. Rev. E **70**, 056223 (2004).

[33] The image data recorded by the camera is processed by frequency filtering with a bandpass filter centered at $f_f/2 = 0.03$ Hz with a width of 0.012 Hz. We treat the resulting signal as $u = ae^{if_f/2}$ and plot the phase of the complex amplitude a. The front line is defined as $\mathrm{Re}(a) = 0$ and the vortex positions are $\mathrm{Re}(a) = \mathrm{Im}(a) = 0$.

[34] The chemical concentrations in the two chemical reserviors separated by the porous membrane were, Reservior I: 0.22 M Malonic acid, 0.2 M Sodium Bromide, 0.184 M potassium bromate, 0.8 M sulfuric acid; Reservior II: 0.184 M potassium bromate, 1×10^{-3} M Tris(2,2'-bipyridyl)dichlororuthenium(II)hexahydrate, 0.8 M sulfuric acid. Each reservior volume is 8.3 ml and the flow rate of chemicals through each Reservior was 20 ml/hr. Chemicals were premixed before entering each reservior; a 10 ml premixer and a 0.5 ml premixer fed Reservior I and II, respectively. The experiments were conducted at room temperature.

[35] A. Hagberg and E. Meron, Phys. Rev. Lett. **78**, 1166 (1997).

[36] A. Hagberg and E. Meron, Phys. Rev. Lett. **91**, 224503 (2003).

[37] Since we do not know how the parameters of Eq. (1) are related to the oscillatory BZ reaction we cannot determine the sign of c/D. The sign, however, is expected to be positive if for $a > a_{nib}$ the Ising front is unstable to transverse perturbations.

[38] A. Hagberg and E. Meron, Physica D **123**, 460 (1998).

[39] P. Coullet, T. Frisch, and G. Sonnino, Phys. Rev. E **49**, 2087 (1994).

[40] A. Yochelis, C. Elphick, A. Hagberg, and E. Meron, Europhys. Lett. **69**, 170 (2005).

[41] J. P. Keener, Stud. Appl. Math **55**, 187 (1976).

[42] H. Kidachi, Prog. Theor. Phys. **63**, 1152 (1980).

[43] A. De Wit, G. Dewel, and P. Borckmans, Phys. Rev. E **48**, R4191 (1993).

[44] A. De Wit, D. Lima, G. Dewel, and P. Borckmans, Phys. Rev. E **54**, 261 (1996).

[45] M. Meixner, A. De Wit, S. Bose, and E. Schöll, Phys. Rev. E **55**, 6690 (1997).

[46] M. Meixner, S. Bose, and E. Schöll, Physica D **109**, 128 (1997).

[47] W. Just, M. Bose, S. Bose, H. Engel, and E. Schöll, Phys. Rev. E **64**, 026219 (2001).